



# Statistical modeling of the fission process of $^{197}\text{Tl}$ , $^{217}\text{Fr}$ , $^{224}\text{Th}$ , and $^{254}\text{Fm}$ nuclei produced in heavy ion reactions within the modified statistical model

H. Eslamizadeh \*

Department of Physics, Faculty of Nano and Bio Science and Technology, Persian Gulf University, 75169 Bushehr, Iran

 (Received 28 February 2024; revised 28 April 2024; accepted 3 June 2024; published 26 June 2024)

Fission processes of the excited compound nuclei  $^{197}\text{Tl}$ ,  $^{217}\text{Fr}$ ,  $^{224}\text{Th}$ , and  $^{254}\text{Fm}$  in a wide range of mass numbers produced in fusion reactions have been simulated in the framework of the modified statistical model and different observables were reproduced for these nuclei. In the statistical calculations have been considered the effects of the projection of the total spin of the compound nucleus onto the symmetry axis  $K$ , the temperature dependence of the location and height of fission transition points, and the classical collective motion of the excited compound nuclei about the ground state. Furthermore, in the present research, particle binding energies as a function of deformation of nuclei and subbarrier fission have been considered for more accurate reproduction of the experimental data. The fission cross section, the evaporation residue cross section, the fission probability, the average pre-scission neutron multiplicity, and the anisotropy of fission fragments' angular distribution have been calculated for the excited compound nuclei  $^{197}\text{Tl}$ ,  $^{217}\text{Fr}$ ,  $^{224}\text{Th}$ , and  $^{254}\text{Fm}$ . In the statistical simulations, the scaling factor of the fission barrier height,  $r_s$ , and the temperature coefficient of the effective potential,  $k$ , were considered as a free parameter. For each reaction the parameters  $r_s$  and  $k$  were adjusted to reproduce a single fission cross section and a single evaporation residue cross section. It was shown that the results of calculations are in good agreement with the experimental data by using appropriate values for these parameters equal to  $k = 0.0182 \pm 0.0050 \text{ MeV}^{-2}$  and  $r_s = 1.0005 \pm 0.0020$  for  $^{197}\text{Tl}$ ;  $k = 0.0063 \pm 0.0040 \text{ MeV}^{-2}$  and  $r_s = 1.0042 \pm 0.0015$  for  $^{217}\text{Fr}$ ;  $k = 0.0060 \pm 0.0040 \text{ MeV}^{-2}$  and  $r_s = 1.0050 \pm 0.0020$  for  $^{224}\text{Th}$ ;  $k = 0.0025 \pm 0.0015 \text{ MeV}^{-2}$  and  $r_s = 1.0100 \pm 0.0014$  for  $^{254}\text{Fm}$ . Furthermore, by using appropriate values of parameters  $k$  and  $r_s$  I have calculated the average pre-scission neutron multiplicity, the fission probability, and the anisotropy of fission fragments' angular distribution for the compound nuclei  $^{197}\text{Tl}$ ,  $^{217}\text{Fr}$ ,  $^{224}\text{Th}$ , and  $^{254}\text{Fm}$ . It was shown that the modified statistical model is well able to reproduce different experimental data, although at high excitation energies the results of calculations for the neutron multiplicity and the anisotropy of fission fragments' angular distribution are slightly lower than the experimental data. It was also shown that, at high excitation energy, for reproducing the neutron multiplicity one needs to increase the nuclear dissipation. Finally, from the comparison of the extracted results of parameters  $k$  and  $r_s$  for the compound nuclei  $^{197}\text{Tl}$ ,  $^{217}\text{Fr}$ ,  $^{224}\text{Th}$ , and  $^{254}\text{Fm}$ , it was shown that the parameter  $k$  decreases and the parameter  $r_s$  increases with increasing mass number of the compound nucleus.

DOI: [10.1103/PhysRevC.109.064624](https://doi.org/10.1103/PhysRevC.109.064624)

## I. INTRODUCTION

The study of the fission of highly excited compound nuclei produced in fusion reactions remains a topic of great interest. Nuclear fission was discovered in December 1938 by chemists Otto Hahn and Fritz Strassmann and physicists Lise Meitner and Otto Robert Frisch [1,2]. After the fission process was discovered, Bohr and Wheeler proposed the standard liquid drop model to describe the fission process of nuclei [3]. Bohr and Wheeler in their model assumed that the compound nucleus is as a mononucleus that equilibrated in all degrees of freedom with no memory of its formation except the conserved quantities such as energy and angular momentum. In this model the fission decay width of a fully equilibrated system can be

determined as follows:

$$\Gamma_f = \frac{N_t}{2\pi\rho}, \quad (1)$$

where  $N_t$  is the number of transition states and  $\rho$  is the total level density of the initial system. By making several simplifying assumptions one can obtain the fission width for a nucleus with total excitation energy  $E^*$  as

$$\Gamma_f = \frac{1}{2\pi} \frac{1}{\rho_{\text{gs}}(E^*)} \int_0^{E^* - B_f} \rho_{\text{sp}}(E^* - B_f - \varepsilon) d\varepsilon, \quad (2)$$

where  $\rho_{\text{gs}}$  and  $\rho_{\text{sp}}$  are the level densities at the ground state and the saddle points, respectively,  $B_f$  is the fission barrier height, and  $\varepsilon$  represents the kinetic energy associated with the fission distortion. The level density of the nuclear system is often estimated assuming a weakly interacting Fermi gas [4]. It should be noted that in very high excitation energy or in a small barrier height the temperatures at the ground and saddle

\*Contact author: [eslamizadeh@pgu.ac.ir](mailto:eslamizadeh@pgu.ac.ir)

points will be equal and so the fission decay width can be considered as

$$\Gamma_f = \frac{T}{2\pi} \exp\left(\frac{-B_f}{T}\right), \quad (3)$$

where  $T$  and  $B_f$  are the temperature of the nucleus and the fission barrier height, respectively. Furthermore, the excitation energy can be low enough and the barrier height large enough such that the temperatures at the ground state and the saddle points are significantly different and so the fission decay width can be given by

$$\Gamma_f = \frac{T_{\text{sp}}}{2\pi} \exp\left(\frac{-2B_f}{T_{\text{gs}} + T_{\text{sp}}}\right), \quad (4)$$

where  $T_{\text{gs}}$  and  $T_{\text{sp}}$  are the temperature of the compound nucleus at the ground and saddle points, respectively. In the fission process the slowing effects of nuclear viscosity can be considered by using the Kramers-modified Bohr and Wheeler model [5]

$$\Gamma_f(K) = (\sqrt{1 + \gamma^2} - \gamma) \frac{\hbar\omega_{\text{eq}}}{2\pi} \exp\left(-\frac{B_f}{T}\right), \quad (5)$$

where  $\gamma$  is the dimensionless nuclear viscosity and can be given by  $\gamma = \beta/2\omega_{\text{sp}}$ ,  $\beta$  is the nuclear dissipation and  $\omega_{\text{eq}}$ ,  $\omega_{\text{sp}}$  are the curvatures of the potential energy surface at the equilibrium and the fission saddle points, respectively.  $B_f$ ,  $\omega_{\text{eq}}$ , and  $\omega_{\text{sp}}$  are all assumed functions of  $K$ . The  $(\sqrt{1 + \gamma^2} - \gamma)$  term is commonly referred to as the Kramers reduction factor. After the Bohr and Wheeler model, many statistical and dynamical model codes were proposed to describe the fission process of nuclei and many papers were published according to these models (see for example Refs. [6–25] and references therein). In many statistical model codes for simulation of the fission process of the excited compound nuclei, a scaling of the fission barrier heights was used and the ratio of the level density parameters at saddle and equilibrium points and magnitude of these parameters was considered as free parameters. The magnitudes of these parameters usually have been adjusted by reproducing different experimental data. It should be mentioned that the fission process of the excited compound nuclei cannot be accurately modeled by using the ratio of the level density parameters at saddle and equilibrium points and the spin dependence of the fission barriers at temperature equal to zero [6]. Furthermore, the curvature at the ground states and the fission transition points and the barrier locations and heights cannot all be determined in a self-consistent manner as a function of spin,  $J$ , projection of spin about the symmetry axis of the nucleus,  $K$ , and temperature of the nucleus. Lestone and McCalla in Ref. [6] introduced a modified statistical model (MSM) and in this model for removing these problems they considered other parameters as free parameters which perform similar roles as a scaling of the fission barrier heights and the ratio of the level density parameters at saddle and equilibrium points. They considered a scaling of the modified liquid drop model (MLDM) radii from their default values to calculate the surface and Coulomb energies with the parameter  $r_s$  and the temperature coefficient in the effective potential formula,  $k$ . In their model, they assumed that

the surface energy is proportional to the square of  $r_s$ , while the Coulomb energy is inversely proportional to  $r_s$ . A value  $r_s = 1$  is the standard MLDM with fission barrier heights in agreement with the finite range liquid drop model (FRLDM). Raising  $r_s$  above 1 decreases the Coulomb energy and increases the surface energy. This causes the fission barriers to increase. It should be mentioned that Lestone and McCalla in Ref. [6] have pointed out that many statistical codes introduced to describe the fission process are missing three pieces of physics. Then, they considered the effects of these pieces of physics in their model. These key pieces of physics are the calculation of the location and height of fission saddle points as a function of excitation energy and the incorporation of the orientation ( $K$  state) degree of freedom and the determination of the total level density of the compound system taking into account the collective motion of the system about the ground state position.

The main purpose of this research is to simulate the fission process of the excited compound nuclei  $^{197}\text{Tl}$ ,  $^{217}\text{Fr}$ ,  $^{224}\text{Th}$ , and  $^{254}\text{Fm}$  produced in  $^{16}\text{O} + ^{181}\text{Ta}$ ,  $^{19}\text{F} + ^{198}\text{Pt}$ ,  $^{16}\text{O} + ^{208}\text{Pb}$ , and  $^{16}\text{O} + ^{238}\text{U}$  reactions, respectively, in the framework of the MSM and determine the appropriate values for the scaling factor of the fission barrier height and the temperature coefficient of the effective potential for these nuclei. It should be mentioned that in the present calculations, particle binding energies as a function of deformation of nuclei and subbarrier fission have been considered for more accurate reproduction of the experimental data.

The present paper has been arranged as follows: The model and basic equations are described in Sec. II. The results of calculations are presented in Sec. III. Finally, the concluding remarks are given in Sec. IV.

## II. DETAILS OF THE MODEL

In a simulation of the fission process a compound nucleus is needed to specify the initial conditions. Generally, the simulation is started at the position of the ground state with a temperature corresponding to the initial excitation energy. The spin value for a compound nucleus can be sampled from a fusion spin distribution. The spin distributions can be determined as in Ref. [26],

$$\frac{d\sigma(J)}{dJ} = \frac{2\pi}{k^2} \frac{2J + 1}{1 + \exp\left(\frac{J - J_c}{\delta J}\right)}, \quad (6)$$

where  $J_c$  is the critical spin and  $\delta J$  is the diffuseness parameter. The parameters  $J_c$  and  $\delta J$  can be determined by relations introduced in Ref. [26]. Figures 1(a) and 1(b) show the spin distributions calculated, for example, for the compound nuclei  $^{224}\text{Th}$  and  $^{254}\text{Fm}$  produced in  $^{16}\text{O} + ^{208}\text{Pb}$  and  $^{16}\text{O} + ^{238}\text{U}$  reactions, for example, for projectile energies equal to  $E_{\text{c.m.}} = 80, 90, 100, 110, 120,$  and  $130$  MeV.

In a simulation of fission process of a compound nucleus, the effective potential energy can be determined by [6]

$$V_{\text{eff}}(q, A, Z, J, K, T) = V(q, A, Z, J, K) - \Delta a(q)T^2, \quad (7)$$

where  $\Delta a$  is equal to the difference in the level density parameter at the saddle point and the equilibrium position and  $V(q, A, Z, J, K)$  is the potential energy. The potential energy

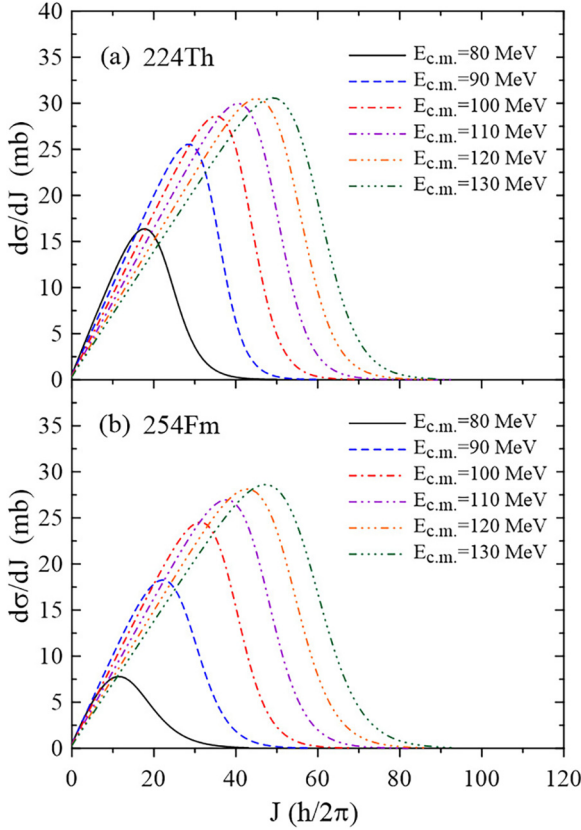


FIG. 1. The spin distributions calculated for the compound nuclei (a)  $^{224}\text{Th}$  and (b)  $^{254}\text{Fm}$  produced in  $^{16}\text{O} + ^{208}\text{Pb}$  and  $^{16}\text{O} + ^{238}\text{U}$  reactions, for example, for projectile energies  $E_{c.m.} = 80, 90, 100, 110, 120$  and  $130$  MeV.

can be calculated as in Refs. [27,28]:

$$V(q, A, Z, J, K) = B_s(q)E_s^0(Z, A) + B_c(q)E_c^0(Z, A) + E_{\text{rot}}, \quad (8)$$

where  $q = r/R_0$  is deformation parameter,  $r$  is the distance between the centers of masses of the future fission fragments, and  $R_0$  is the radius of the spherical nucleus.  $A$  and  $z$  are mass and atomic numbers of the nucleus, respectively.  $J$  and  $K$  are spin and projection of spin about the symmetry axis of the nucleus, respectively.  $B_c(q)$  and  $B_s(q)$  are Coulomb and surface energy terms, respectively.  $E_s^0$  and  $E_c^0$  are, respectively, the surface and Coulomb energies of the corresponding spherical system as determined by Myers and Swiatecki [29,30]. In Eq. (8)  $E_{\text{rot}}$  is the rotational energy and can be determined by

$$E_{\text{rot}} = \frac{\hbar^2 J(J+1)}{2I_{\perp}(q)} + \frac{\hbar^2 K^2}{2I_{\parallel}(q)}, \quad (9)$$

where  $I_{\text{eff}}$  is the effective moment of inertia. The inverse of the effective moment of inertia is  $I_{\text{eff}}^{-1} = I_{\parallel}^{-1} - I_{\perp}^{-1}$ .  $I_{\parallel}$  and  $I_{\perp}$  are the momenta of inertia parallel and perpendicular to the symmetry axis of the fissioning nucleus.

It should be mentioned that the Fermi-gas level density parameter  $a$  is independent of the nuclear shape. However, for real nuclei the level density parameter is expected to have a

dependence on nuclear shape. If the level-density parameter is assumed to be as

$$a(q) = a_v A + a_s A^{2/3} B_s(q), \quad (10)$$

then the effective potential can be obtained using a  $(1 - kT^2)$  dependence of the surface energy [6],

$$V_{\text{eff}}(q, A, Z, J, K, T) = B_s(q)E_s^0(Z, A)(1 - kT^2) + B_c(q)E_c^0(Z, A) + E_{\text{rot}}, \quad (11)$$

where  $k = c_s A^{2/3}/E_s^0$ . Töke and Swiatecki [31] obtain  $c_s \approx 0.27$  and other estimates of  $c_s$  give values of  $k$  that range  $0.007-0.022 \text{ MeV}^{-2}$  [4,32–35]. It should be stressed that  $c_s$  is very sensitive to the assumed properties of nuclear matter and to other approximations [35]. In Eq. (10)  $B_s(q)$  is the surface energy in the liquid drop model and  $A$  is the mass number of the compound nucleus. In Eq. (10) the values of the parameters  $a_v = 0.073 \text{ MeV}^{-1}$  and  $a_s = 0.095 \text{ MeV}^{-1}$  are taken from the work of Ignatyuk *et al.* [4]. Figures 2(a)–2(c) show the effective potential calculated, for example, for the compound nucleus  $^{224}\text{Th}$  produced in the  $^{16}\text{O} + ^{208}\text{Pb}$  reaction as a function of the coordinate  $q$  and different combination of  $J$ ,  $K$ , and  $T$ . It is clear from Figs. 2(a) and 2(b) that the height of the effective potential,  $B_f$ , decreases with increasing spin of nucleus and also for a given value of spin the height of the effective potential increases with increasing the value of  $K$ . It is also clear from Fig. 2(c) that the effective potential decreases with increasing temperature. Figure 3 also shows the effective potential at  $T = 1.5 \text{ MeV}$  and  $J = 30\hbar$  for the compound nucleus  $^{224}\text{Th}$  as a function of the coordinates  $q$  and  $K$ .

In simulation of the fission process of a compound nucleus, the time evolution is followed over small time steps, and the fate of the system at each time step is decided by a Monte Carlo sampling of the decay widths of various channels. In other words, at each time step are calculated the decay widths for emission of light particles  $n, p, \alpha, \gamma$  and the decay width for the fission event. Furthermore, the probabilities of decay via different channels can be calculated by using a standard Monte Carlo cascade procedure where the kind of decay selected with the weights  $\Gamma_v/\Gamma_{\text{tot}}$  ( $v = n, p, \alpha, \gamma, \text{fission}$ ) and  $\Gamma_{\text{tot}} = \Gamma_n + \Gamma_p + \Gamma_\alpha + \Gamma_\gamma + \Gamma_f$ . This procedure simulates the law for radioactive decay for the different particles. This procedure allows for multiple emissions of light particles and a higher chance of fission. The loss of angular momentum is taken into account by assuming that a neutron carries away  $1\hbar$ , a proton  $1\hbar$ , an  $\alpha$  particle  $2\hbar$ , and a  $\gamma$  quantum  $1\hbar$ . After each emission act of a particle of kind  $v = n, p, \alpha, \gamma$  the kinetic energy of the emitted particle is calculated by a hit and miss Monte Carlo procedure. The particle decay width of a particle of kind  $v$  can be calculated as in Ref. [36],

$$\Gamma_v(E^*, J) = \frac{(2s_v + 1)}{2\pi \rho_c(E^*, J)} \times \int_0^{E^* - B_v} \sum_l T_l(\varepsilon_v) \times \sum_{I=|J-l|}^{I=|J+l|} \rho_R(E^* - B_v - \varepsilon_v, I) d\varepsilon_v, \quad (12)$$

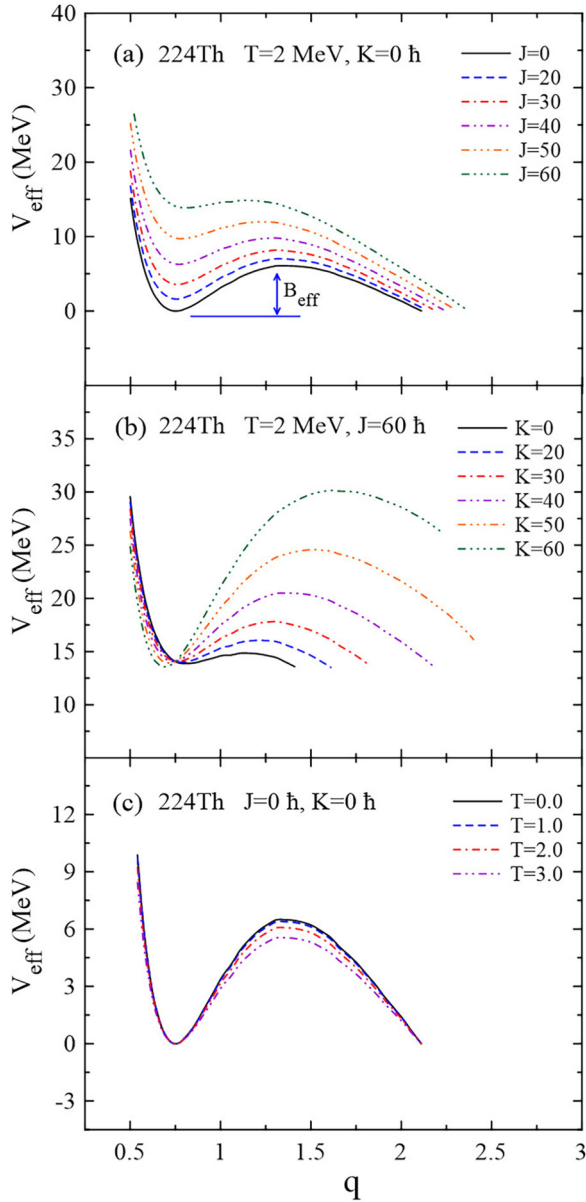


FIG. 2. The effective potential for the compound nucleus  $^{224}\text{Th}$  produced in  $^{16}\text{O} + ^{208}\text{Pb}$  reaction as a function of the coordinate  $q$  for (a) different values of  $J$  at  $T = 2$  MeV and  $K = 0\hbar$ , (b)  $J = 60\hbar$ ,  $T = 2$  MeV and different values of  $K$ , and (c)  $J = 0\hbar$ ,  $K = 0\hbar$  and different values of  $T$ .  $B_f$  is the effective fission barrier height.

where  $\varepsilon$ ,  $s_v$ , and  $l$  are the kinetic energy, spin, and orbital angular momentum of the emitted particle,  $B_v$  is the liquid drop binding energies of the emitted particle  $v$ ,  $\rho_c$  and  $\rho_R$  are the level densities of the compound and residual nuclei, and  $T_l$  is the transmission coefficient. Particle binding energies as a function of deformation can be calculated by

$$B_v(q) = M_p(q) - M_d(q) - M_v, \quad (13)$$

where  $M_v$  with  $v = n, p, \alpha$  is the mass of the emitted particle.  $M_p(q)$  and  $M_d(q)$  are the masses of the mother and daughter nuclei, respectively. The mass of a deformed nucleus is determined in terms of the Coulomb energy  $B_c(q)$  and the surface

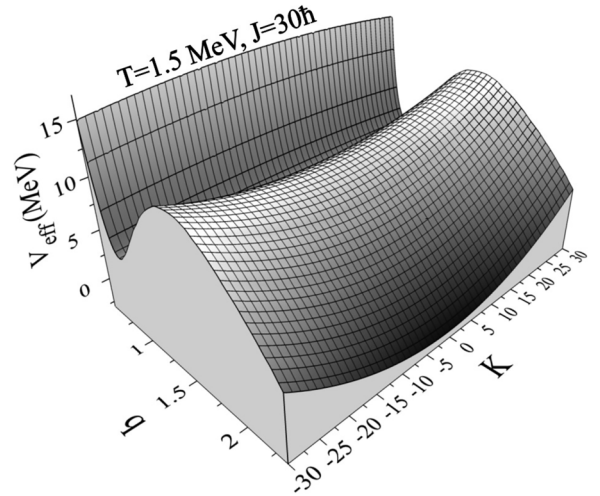


FIG. 3. The effective potential at  $T = 1.5$  MeV and  $J = 30\hbar$  for the compound nucleus  $^{224}\text{Th}$  produced in  $^{16}\text{O} + ^{208}\text{Pb}$  reaction as a function of the coordinates  $q$  and  $K$ .

energy  $B_s(q)$ . The deformation dependence of the charged-particle emission barriers can be determined as in Ref. [26] by  $V_c(q) = V_v B_c(q)$ , where  $V_v = [(Z - Z_v)Z_v K_v] / (R_v + 1.6)$  with  $K_v = 1.15$  for protons and 1.32 for  $\alpha$  particles.  $R_v = 1.21[(A - A_v)^{1/3} + A_v^{1/3}] + (3.4/\varepsilon_v^{1/2})\delta_{v,n}$ , where  $A_v$  and  $\varepsilon_v$  are the mass number and the kinetic energy of the emitted particle  $v = n, p, \alpha$ . Figure 4 shows the change in neutron, proton, and  $\alpha$ -particle binding energies as a function of  $q$  relative to the spherical binding energies, for example, for the compound nucleus  $^{224}\text{Th}$ . It is clear from Fig. 4 that the neutron binding energies decreases slightly while the proton and alpha particle binding energies increase rapidly with deformation. Such behavior is expected, because for a fixed deformation the removal of a neutron causes a slight decrease in the nuclear deformation energy, while the removal of charges causes a rapid increase. It should be noted that the charged particles' emission probability decreases with

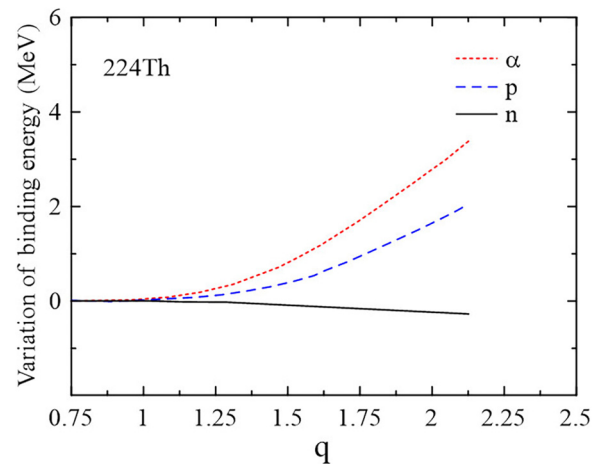


FIG. 4. Variation of binding energy of neutron, proton, and  $\alpha$  particle as a function of  $q$  relative to the spherical binding energies for the compound nucleus  $^{224}\text{Th}$ .



increasing deformation of the compound nucleus  $^{224}\text{Th}$ . Consequently, the neutron emission probability increases relative to the charged particle emission probability.

The  $\gamma$ -ray decay width at each time step is calculated as in Ref. [37],

$$\Gamma_\gamma \cong \frac{3}{\rho_c(E_{\text{int}})} \int_0^{E_{\text{int}}} d\varepsilon \rho_c(E_{\text{int}} - \varepsilon) f(\varepsilon), \quad (14)$$

where  $\varepsilon$  is the energy of the emitted  $\gamma$ -ray and  $f(\varepsilon)$  is calculated by

$$f(\varepsilon) = \frac{4}{3\pi} \frac{e^2}{\hbar c} \frac{1+kNZ}{mc^2} \frac{\Gamma_G \varepsilon^4}{(\Gamma_G \varepsilon)^2 + (\varepsilon^2 - E_G^2)^2}, \quad (15)$$

with  $\Gamma_G = 5$  MeV,  $E_G = 80 A^{-1/3}$ ,  $k = 0.75$  [38], and  $\Gamma_G$  and  $E_G$  are the width and position of the giant dipole resonance, respectively. The intrinsic excitation energy for a rotating system can be given by

$$E_{\text{int}} = E^* - V_{\text{eff}}(q) - E_{\text{rot}}. \quad (16)$$

The fission decay width for a system with fixed spin  $K$  about the symmetry axis can be determined by Eq. (5). The full fission decay width can be obtained by summing over all possible  $K$  [6],

$$\Gamma_f = \frac{\sum_{K=-J}^J P(K) \Gamma_f(K)}{\sum_{K=-J}^J P(K)}, \quad (17)$$

where  $P(K)$  is the probability that the system is in a given  $K$  and it can be determined by

$$P(K) = \frac{T}{\hbar \omega_{\text{eq}}} \exp\left(-\frac{V_{\text{eq}}}{T}\right), \quad (18)$$

where  $V_{\text{eq}}$  is the potential energy at the equilibrium position.

It should be mentioned that in the present research tunneling effects have been also considered for description of the fission process of nuclei, when the energy of the compound system is smaller than the energy of the fission barrier, because the tunneling effect plays an important role in this energy region. The subbarrier fission decay width for nuclei can be determined as in Ref. [19]. The level density of a spherical system and a deformed system can be determined as in Ref. [6]

Figure 5 shows the  $n$ ,  $p$ ,  $\alpha$ ,  $\gamma$  and fission decay widths as a function of excitation energy calculated, for example, for the compound nuclei  $^{224}\text{Th}$  and  $^{254}\text{Fm}$ . It can be seen from Fig. 5 that the decay widths are rapidly increased by excitation energies in the range of  $E^* < 40$  MeV. It is also observed that the neutron widths are also larger than those of the proton and alpha emissions.

In the present statistical model, the fission cross section is determined in terms of the fusion cross section,

$$\sigma_{\text{Fiss}} = \sum_J \sigma_{\text{Fus}}(J) \frac{\Gamma_f}{\Gamma_{\text{tot}}}. \quad (19)$$

The total fusion cross section can be calculated from

$$\sigma_{\text{Fus}} = \sum_J \frac{d\sigma_{\text{Fus}}(J)}{dJ}, \quad (20)$$

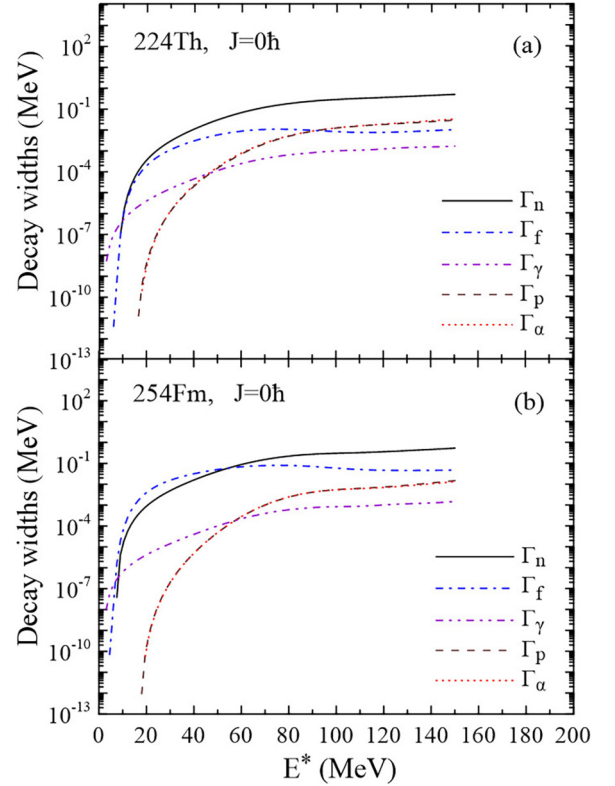


FIG. 5. Comparisons of the decay widths of the light particle emissions and the fission width as a function of excitation energy calculated for the compound nuclei (a)  $^{224}\text{Th}$  and (b)  $^{254}\text{Fm}$ .

where the spin distribution of the compound nucleus can be considered by Eq. (6). The fission probability  $P_f$  can also be calculated by the relation  $P_f = N_{\text{fiss}}/(N_{\text{fiss}} + N_{\text{eva}})$  where  $N_{\text{fiss}}$  is the number of fission events and  $N_{\text{eva}}$  is the number of evaporation residue events.

The anisotropy of fission fragment angular distribution can be calculated in the framework of the saddle point transition model (SPTS) [39–42]. In analyzing the fission fragment angular distributions, it is usually assumed that fission fragments travel in the direction of the symmetry axis of the nucleus. Consequently, the fission fragment angular distributions can be determined by three quantum numbers:  $J, M, K$ , where  $J$  is the spin of a compound nucleus,  $M$  is the projection of  $J$  on the axis of the projectile ion beam, and  $K$  is the projection of  $J$  on the symmetry axis of the nucleus. In the case of fusion of spinless ions, the magnitude of  $M$  is equal to zero. At fixed values of  $J$  and  $K$ , the angular distribution can be determined as follows:

$$W(\theta, J, K) = (J + 1/2) |d_{M=0, K}^J(\theta)|^2, \quad (21)$$

where  $\theta$  is the angle between the beam axis and the nuclear symmetry axis and function  $d_{M, K}^J(\theta)$  can be defined as in Ref. [40]. At high values of  $J$ ,  $W(\theta, J, K)$  can be approximated as

$$W(\theta, J, K) \approx \frac{J + 1/2}{\pi} [(J + 1/2)^2 \sin^2 \theta - K^2]^{1/2}. \quad (22)$$

The fission fragments' angular distribution can be calculated by averaging Eq. (22) over the quantum numbers  $J$  and  $K$  as follows:

$$W(\theta) = \sum_{J=0}^{\infty} \sigma_J \sum_{K=-J}^J P(K)W(\theta, J, K), \quad (23)$$

where  $P(K)$  is the distribution of the compound nuclei over  $K$ . In the SPTS model this function can be determined by the Boltzmann factor  $\exp(-E_{rot}/T)$  [42] at the saddle point. Therefore, the equilibrium distribution with respect to  $K$  can be expressed as

$$P_{eq}(K) = \frac{\exp[-K^2/(2K_0^2)]}{\sum_{K=-J}^J \exp[-K^2/(2K_0^2)]}, \quad (24)$$

where variance of the equilibrium  $K$  distribution,  $K_0$ , is given by the expression  $K_0^2 = (T/\hbar^2)I_{eff}$  where  $T$  is the nuclear temperature. It can be shown that the anisotropy of fission fragment angular distribution can be given by the approximate relation

$$A = \frac{\langle W(180^\circ) \rangle}{\langle W(90^\circ) \rangle} \approx 1 + \frac{\langle J^2 \rangle}{4K_0^2}. \quad (25)$$

### III. RESULTS AND DISCUSSION

In the framework of the MSM have been simulated fission process of the excited compound nuclei  $^{197}\text{Tl}$ ,  $^{217}\text{Fr}$ ,  $^{224}\text{Th}$ , and  $^{254}\text{Fm}$  produced in  $^{16}\text{O} + ^{181}\text{Ta}$ ,  $^{19}\text{F} + ^{198}\text{Pt}$ ,  $^{16}\text{O} + ^{208}\text{Pb}$ , and  $^{16}\text{O} + ^{238}\text{U}$  reactions, respectively. The fission cross section, the evaporation residue cross section, the fission probability, the average pre-scission neutron multiplicity, and the anisotropy of fission fragments' angular distribution have been calculated for the excited compound nuclei  $^{197}\text{Tl}$ ,  $^{217}\text{Fr}$ ,  $^{224}\text{Th}$ , and  $^{254}\text{Fm}$ . It should be mentioned that in the present calculations, particle binding energies as a function of deformation of nuclei and subbarrier fission have been considered for more accurate reproduction of the experimental data. In the statistical calculations, the nuclear dissipation is considered equal to  $3 \times 10^{21} \text{ s}^{-1}$ , a value that is consistent with theoretical and experimental estimates [26,43,44]. Furthermore, in the calculations the parameters  $k$  and  $r_s$  are adjusted to reproduce a single fission and residue cross sections. Figures 6(a), 6(b), 7(a), 7(b), 8(a), 8(b), 9(a), and 9(b) show the results of the calculations for the fission and evaporation residue cross sections and the cross sections for the formation of evaporation residues in the  $2n$ ,  $3n$ ,  $4n$ , and  $5n$  channels in  $^{16}\text{O} + ^{181}\text{Ta}$ ,  $^{19}\text{F} + ^{198}\text{Pt}$ ,  $^{16}\text{O} + ^{208}\text{Pb}$ , and  $^{16}\text{O} + ^{238}\text{U}$  reactions.

It can be seen from Figs. 6(a), 6(b), 7(a), 7(b), 8(a), 8(b), 9(a), and 9(b) that the results of the calculations are in good agreement with the experimental data by using values of  $k = 0.0182 \pm 0.0050 \text{ MeV}^{-2}$  and  $r_s = 1.0005 \pm 0.0020$  for  $^{197}\text{Tl}$ ;  $k = 0.0063 \pm 0.0040 \text{ MeV}^{-2}$  and  $r_s = 1.0042 \pm 0.0015$  for  $^{217}\text{Fr}$ ;  $k = 0.0060 \pm 0.0040 \text{ MeV}^{-2}$  and  $r_s = 1.0050 \pm 0.0020$  for  $^{224}\text{Th}$ ;  $k = 0.0025 \pm 0.0015 \text{ MeV}^{-2}$  and  $r_s = 1.0100 \pm 0.0014$  for  $^{254}\text{Fm}$ . It is clear from Figs. 6(a), 7(a), 8(a), and 9(a) that at higher projectile energies the fission cross section reaches a constant value. This is because with increasing projectile energy the pre-scission particle multiplicity

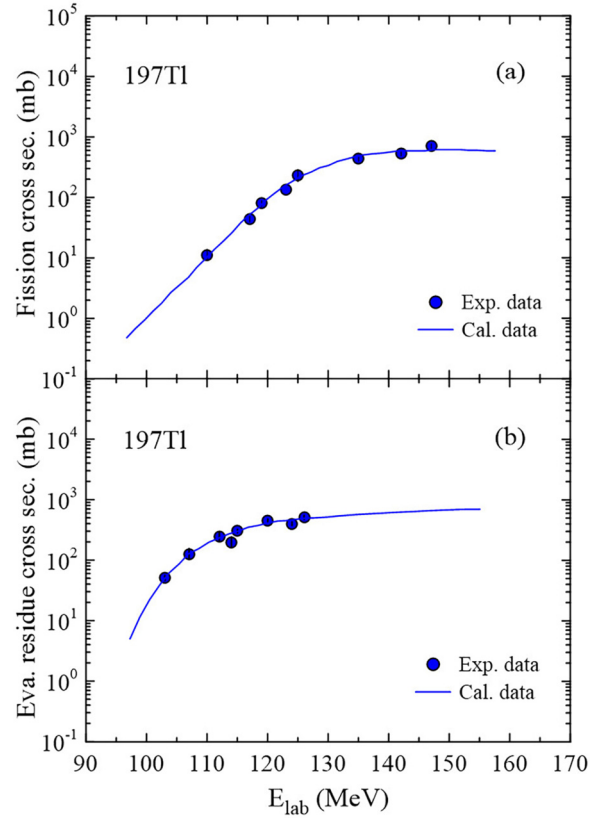


FIG. 6. The results of (a) the fission cross section and (b) the evaporation residues cross section for the  $^{16}\text{O} + ^{181}\text{Ta}$  reaction calculated considering  $k = 0.0182 \pm 0.0050 \text{ MeV}^{-2}$  and  $r_s = 1.0005 \pm 0.0020$ . The solid symbols are experimental data [45–47].

increases and each emission of a light particle carries away angular momentum and excitation energy, therefore fission barrier height of the residual nucleus increases and consequently the fission event becomes less and less probable.

In the present research, the average pre-scission neutron multiplicity, the anisotropy of fission fragments angular distribution, and the fission probability have been calculated for the excited compound nuclei  $^{197}\text{Tl}$ ,  $^{217}\text{Fr}$ ,  $^{224}\text{Th}$ , and  $^{254}\text{Fm}$  to evaluate the estimated values for the parameters  $k$  and  $r_s$ . Figures 10(a)–10(d) show the results of the calculations for the average pre-scission neutron multiplicities for the nuclei  $^{197}\text{Tl}$ ,  $^{217}\text{Fr}$ ,  $^{224}\text{Th}$ , and  $^{254}\text{Fm}$ . It is clear from Figs. 10(a)–10(d) that the experimental data of the neutron multiplicities for the nuclei  $^{197}\text{Tl}$ ,  $^{217}\text{Fr}$ ,  $^{224}\text{Th}$ , and  $^{254}\text{Fm}$  can be satisfactorily reproduced by considering appropriate values for the parameters  $k$  and  $r_s$ , although at high excitation energies the results of calculations are slightly lower than the experimental data. This is probably due to the compound nuclei at high excitation energy being formed with a larger value of spin and temperature, thus the fission barrier height will be reduced [see Figs. 2(a) and 2(c)] and therefore the neutron multiplicities are slightly reduced. For reproducing experimental data of the neutron multiplicities at high excitation energy, the magnitude of the nuclear dissipation can be increased.

It is clear from Figs 10(a)–10(d) that the experimental data at high excitation energy can be reproduced by using

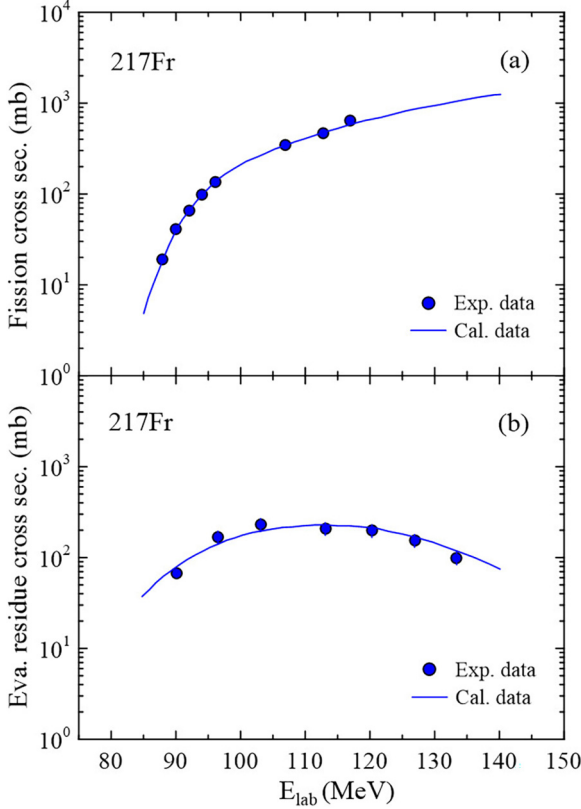


FIG. 7. The results of (a) the fission cross section and (b) the evaporation residues cross section for the  $^{19}\text{F} + ^{198}\text{Pt}$  reaction calculated considering  $k = 0.0063 \pm 0.0040 \text{ MeV}^{-2}$  and  $r_s = 1.0042 \pm 0.0015$ . The solid symbols are experimental data [48,49].

the magnitude of nuclear dissipation equal to  $5 \times 10^{21} \text{ s}^{-1}$ . It should be noted that using appropriate values for the parameters  $k$  and  $r_s$  is very important for reproducing experimental data. The importance of considering these parameters in calculations can be investigated by reproducing experimental data by using  $k = 0$  and  $r_s = 1$ . In Figs. 10(a)–10(d), the results of calculations for precession neutron multiplicity calculated by using  $k = 0$  and  $r_s = 1$  were also included. It is clear from Figs. 10(a)–10(d) that by using  $k = 0$  and  $r_s = 1$  the experimental data on precession neutron multiplicity cannot be reproduced satisfactorily, and the amounts of computational data for  $^{197}\text{Tl}$ ,  $^{217}\text{Fr}$ ,  $^{224}\text{Th}$ , and  $^{254}\text{Fm}$  are less than the experimental data. Figures 11(a), 11(b), and 12 also show the results of anisotropy of the fission fragment angular distribution as a function of projectile energy and scattering angle for  $^{224}\text{Th}$  and  $^{254}\text{Fm}$  nuclei.

It can be seen from Figs 11(a), 11(b), and 12 that the difference between the calculated data and experimental data calculated by using appropriate values of the parameters  $k$  and  $r_s$  is small, although at higher projectile energies the calculated data are slightly lower than the experimental data.

In the present investigation the fission probability has been also calculated for the excited compound nucleus  $^{224}\text{Th}$  with considering  $k = 0.0060 \pm 0.0040 \text{ MeV}^{-2}$  and  $r_s = 1.0050 \pm 0.0020$ . Figure 13 shows the fission probability for  $^{224}\text{Th}$  as a function of excitation energy. It can be seen from Fig. 13

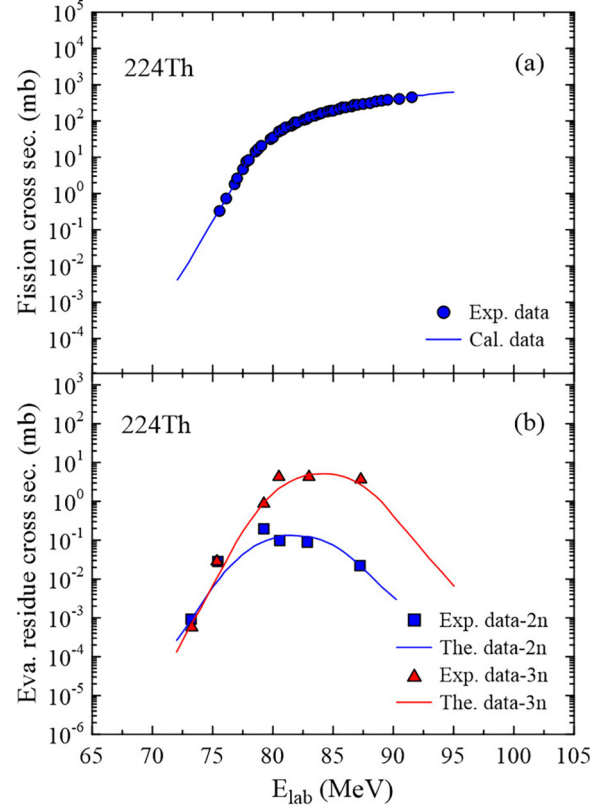


FIG. 8. The results of (a) the fission cross section and (b) the cross section for the formation of evaporation residues in the  $2n$  and  $3n$  channels in the  $^{16}\text{O} + ^{208}\text{Pb}$  reaction calculated considering  $k = 0.0060 \pm 0.0040 \text{ MeV}^{-2}$  and  $r_s = 1.0050 \pm 0.0020$ . The solid symbols are experimental data [50,51].

that the calculated data calculated by using appropriate values for the parameters  $k$  and  $r_s$  satisfactorily reproduced the experimental data.

It is clear from Fig. 13 that at low excitation energies the results of calculation are slightly lower than the experimental data. This could probably be due to not considering shell effects in the present calculations.

Finally, it would be useful to compare the extracted values of the parameters  $k$  and  $r_s$  for the compound nuclei  $^{197}\text{Tl}$ ,  $^{217}\text{Fr}$ ,  $^{224}\text{Th}$ , and  $^{254}\text{Fm}$  which are studied in the present research. Figures 14(a) and 14(b) show the extracted values of the parameters  $k$  and  $r_s$  as a function of compound nucleus mass number. It is clear from Fig. 14 that the parameter  $k$  decreases and the parameter  $r_s$  increases with increasing mass number of the compound nucleus.

#### IV. CONCLUSIONS

In the framework of the MSM have been simulated the fission process of the excited compound nuclei  $^{197}\text{Tl}$ ,  $^{217}\text{Fr}$ ,  $^{224}\text{Th}$ , and  $^{254}\text{Fm}$  produced in  $^{16}\text{O} + ^{181}\text{Ta}$ ,  $^{19}\text{F} + ^{198}\text{Pt}$ ,  $^{16}\text{O} + ^{208}\text{Pb}$ , and  $^{16}\text{O} + ^{238}\text{U}$  reactions, respectively. The effects of the projection of the total spin of the compound nucleus onto the symmetry axis, the temperature dependence of the location and height of fission transition points, and the classical collective motion of the excited

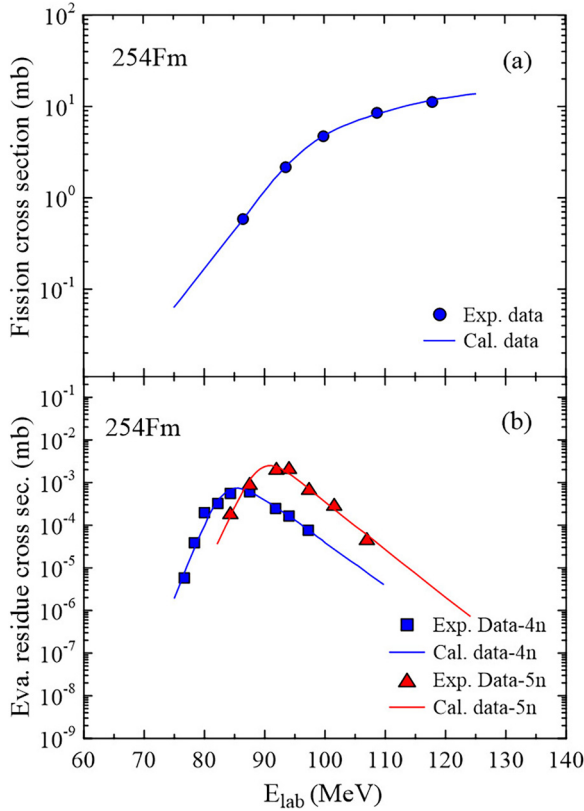


FIG. 9. The results of (a) the fission cross section and (b) the cross section for the formation of evaporation residues in the  $4n$  and  $5n$  channels in the  $^{16}\text{O} + ^{238}\text{U}$  reaction calculated considering  $k = 0.0025 \pm 0.0015 \text{ MeV}^{-2}$  and  $r_s = 1.0100 \pm 0.0014$ . The solid symbols are experimental data [52,53].

compound nuclei about the ground state have been considered in the statistical calculations. Furthermore, in the present research particle binding energies as a function of deformation of nuclei and subbarrier fission have been considered for more accurate reproduction of the experimental data. In the statistical calculations, the temperature coefficient of the effective potential and the scaling factor of the fission barrier height were considered as a free parameter and their magnitudes were adjusted to reproduce a single fission cross section and a single evaporation residue cross section. It was shown that appropriate values for the temperature coefficient of the effective potential and the scaling factor of the fission barrier height for the excited compound nuclei  $^{197}\text{Tl}$ ,  $^{217}\text{Fr}$ ,  $^{224}\text{Th}$ , and  $^{254}\text{Fm}$  are equal to  $k = 0.0182 \pm 0.0050 \text{ MeV}^{-2}$  and  $r_s = 1.0005 \pm 0.0020$  for  $^{197}\text{Tl}$ ;  $k = 0.0063 \pm 0.0040 \text{ MeV}^{-2}$  and  $r_s = 1.0042 \pm 0.0015$  for  $^{217}\text{Fr}$ ;  $k = 0.0060 \pm 0.0040 \text{ MeV}^{-2}$  and  $r_s = 1.0050 \pm 0.0020$  for  $^{224}\text{Th}$ ;  $k = 0.0025 \pm 0.0015 \text{ MeV}^{-2}$  and  $r_s = 1.0100 \pm 0.0014$  for  $^{254}\text{Fm}$ . In the present research, the average precession neutron multiplicity, the anisotropy of fission fragments angular, and the fission probability have been calculated for the excited compound nuclei  $^{197}\text{Tl}$ ,  $^{217}\text{Fr}$ ,  $^{224}\text{Th}$ , and  $^{254}\text{Fm}$  to evaluate the estimated values for the parameters of  $k$  and  $r_s$ . Comparison of the calculations data with the experimental data has shown that

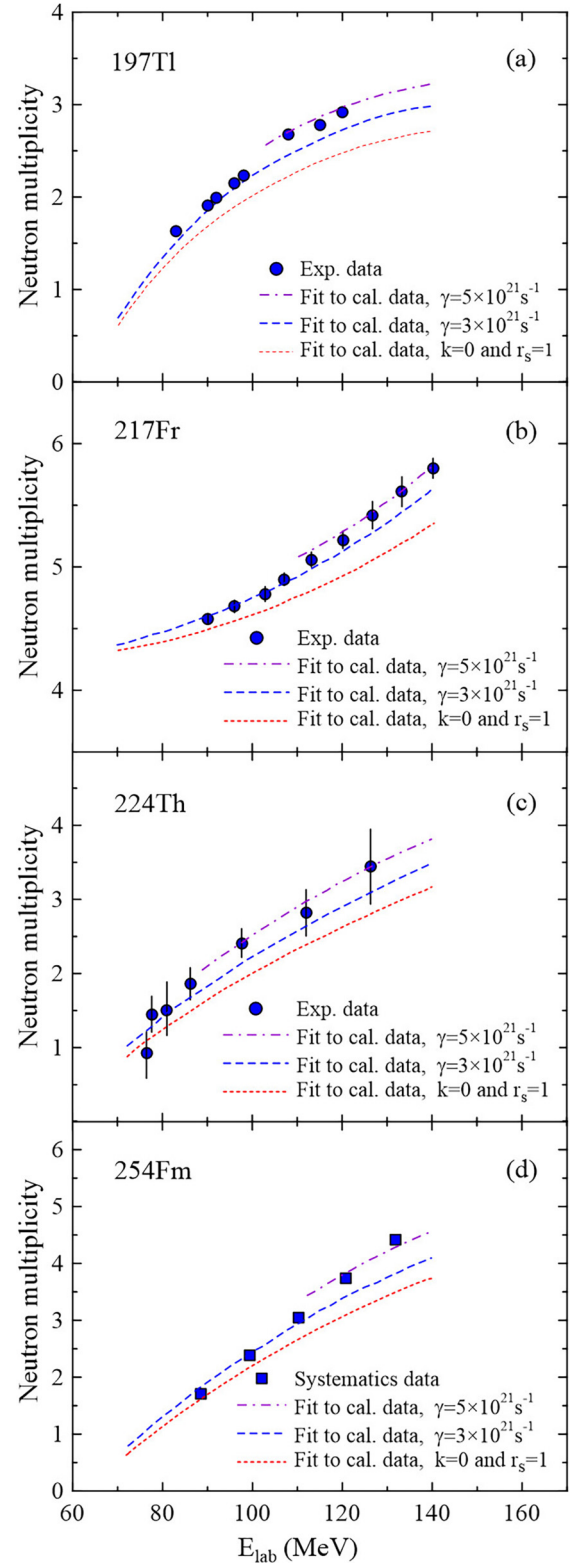


FIG. 10. The results of the pre-fission neutron multiplicities as a function of projectile energy for the excited compound nuclei  $^{197}\text{Tl}$ ,  $^{217}\text{Fr}$ ,  $^{224}\text{Th}$ , and  $^{254}\text{Fm}$  calculated considering appropriate values for the parameters  $k$  and  $r_s$  (dashed lines) and considering  $k = 0$  and  $r_s = 1$  (dotted lines). The solid circles are experimental data [54–56] and the solid squares are the results of calculations based on the systematics [57].



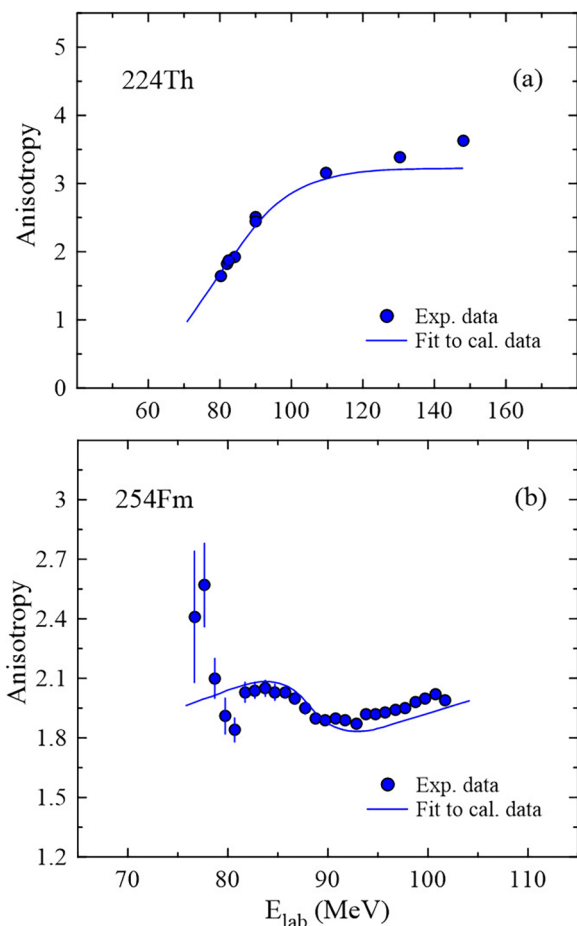


FIG. 11. The results of anisotropy of the fission fragment angular distribution as a function of projectile energy for the compound nuclei (a)  $^{224}\text{Th}$  and (b)  $^{254}\text{Fm}$ . The solid circles are experimental data [50,52,58–60].

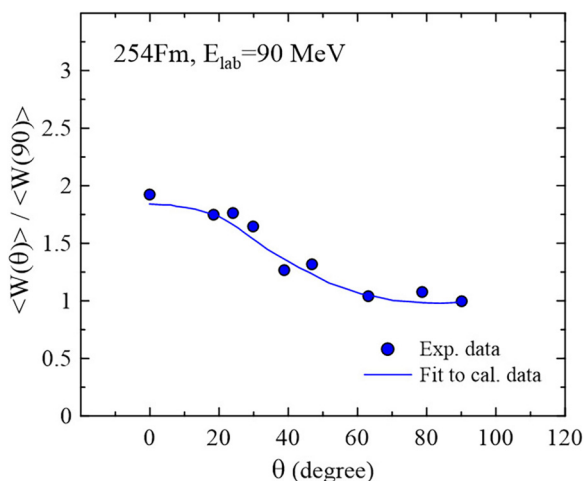


FIG. 12. The results of fission fragment angular distributions as a function of scattering angle at bombarding energy  $E_{\text{lab}} = 90$  MeV for the excited compound nucleus  $^{254}\text{Fm}$ . The filled circles are experimental data [52].

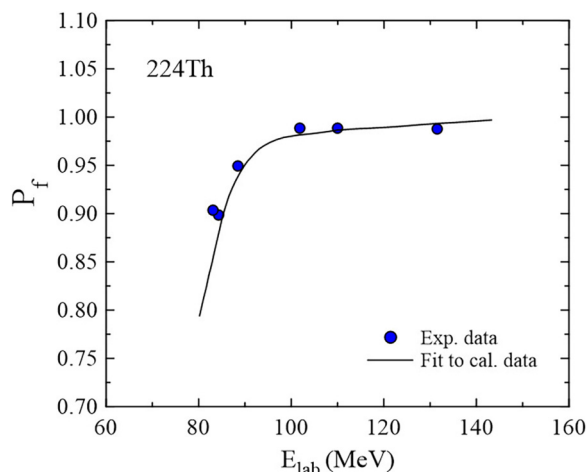


FIG. 13. The results of fission probability as a function of excitation energy for the compound nucleus  $^{224}\text{Th}$ . The solid circles are experimental data [52,61].

the MSM is well able to reproduce the experimental data for the excited compound nuclei  $^{197}\text{Tl}$ ,  $^{217}\text{Fr}$ ,  $^{224}\text{Th}$ , and  $^{254}\text{Fm}$  by using appropriate values for the parameters  $k$  and  $r_s$ , although at high excitation energies the results of calculations for the neutron multiplicity and the anisotropy of fission fragments angular distribution are slightly lower than the experimental data. Furthermore, at low excitation energies

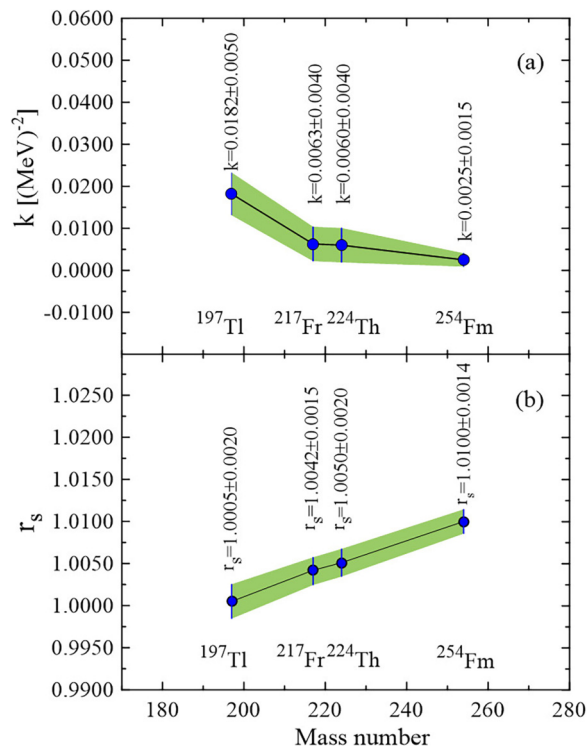


FIG. 14. The extracted values of the parameters  $k$  and  $r_s$  for the compound nuclei  $^{197}\text{Tl}$ ,  $^{217}\text{Fr}$ ,  $^{224}\text{Th}$ , and  $^{254}\text{Fm}$  (solid circles). The shaded areas represent the variation of the parameters  $k$  and  $r_s$  with the compound nucleus mass number.

the results of calculations for fission probability were also slightly lower than the experimental data. Finally, from the comparison of the extracted results of parameters  $k$  and  $r_s$  for the compound nuclei  $^{197}\text{Tl}$ ,  $^{217}\text{Fr}$ ,  $^{224}\text{Th}$ , and  $^{254}\text{Fm}$ , it was shown that the parameter  $k$  decreases and the parameter  $r_s$  increases with increasing mass number of the compound nucleus.

## ACKNOWLEDGMENTS

The author thanks the anonymous referee for comments and suggestions, which led to a significantly improved version of this paper. Support from the Research Committee of the Persian Gulf University is greatly acknowledged.

- 
- [1] O. Hahn and F. Strassmann, *Naturwissenschaften* (1913-2014) **27**, 11 (1939); **27**, 89 (1939); **27**, 163 (1939).
- [2] L. Meitner and O. R. Frisch, *Nature (London)* **143**, 471 (1939).
- [3] N. Bohr and J. A. Wheeler, *Phys. Rev.* **56**, 426 (1939).
- [4] A. V. Ignatyuk, M. G. Itkis, V. N. Okolovich, G. N. Smirenkin, and A. S. Tishin, *Yad. Fiz.* **21**, 1185 (1975).
- [5] H. A. Kramers, *Physica (Amsterdam)* **7**, 284 (1940).
- [6] J. P. Lestone and S. G. McCalla, *Phys. Rev. C* **79**, 044611 (2009).
- [7] M. Blann and T. A. Komoto, Hauser Feshbach codes for nuclei at high excitation and angular momenta, Lawrence Livermore National Laboratory Report No. UCID 19, 1982.
- [8] M. Blann and J. Bisplinghoff, Code A1ICE/LIVERMORE 82 Lawrence Livermore National Laboratory Report No. UCID 19614, 1982.
- [9] H. Rossner, D. Hilscher, D. J. Hinde, B. Gebauer, M. Lehmann, M. Wilpert, and E. Mordhorst, *Phys. Rev. C* **40**, 2629 (1989).
- [10] A. Gavron, *Phys. Rev. C* **21**, 230 (1980).
- [11] H. Eslamizadeh and E. Ahadi, *Phys. Rev. C* **96**, 034621 (2017).
- [12] H. Eslamizadeh, *Phys. Rev. C* **94**, 044610 (2016).
- [13] M. D. Usang, F. A. Ivanyuk, C. Ishizuka, and S. Chiba, *Sci. Rep.* **9**, 1525 (2019).
- [14] N. Kumari, A. Deep, and R. Kharab, *Phys. Rev. C* **105**, 014628 (2022).
- [15] R. Kaur, M. Kaur, and S. Pal, *Phys. Rev. C* **106**, 024604 (2022).
- [16] H. Eslamizadeh and H. Raanaei, *Ann. Nucl. Energy* **51**, 252 (2013).
- [17] H. Eslamizadeh, *Pramana, J. Phys.* **80**, 621 (2013).
- [18] T. L. Zhao and X. J. Bao, *Phys. Rev. C* **98**, 064307 (2018).
- [19] V. Yu. Denisov and I. Yu. Sedykh, *Eur. Phys. J. A* **54**, 231 (2018).
- [20] H. Eslamizadeh, *Pramana, J. Phys.* **78**, 231 (2012).
- [21] H. Eslamizadeh, *Ann. Nucl. Energy* **38**, 2806 (2011).
- [22] K. H. Schmidt and B. Jurado, *Rep. Prog. Phys.* **81**, 106301 (2018).
- [23] W. Ye and N. Wang, *Phys. Rev. C* **106**, 034603 (2022).
- [24] H. Eslamizadeh, *Eur. Phys. J. A* **50**, 1 (2014).
- [25] H. Eslamizadeh, *J. Phys. G: Nucl. Part. Phys.* **40**, 095102 (2013).
- [26] P. Fröbrich and I. I. Gontchar, *Phys. Rep.* **292**, 131 (1998).
- [27] J. P. Lestone, *Phys. Rev. C* **59**, 1540 (1999).
- [28] J. P. Lestone, *Phys. Rev. C* **51**, 580 (1995).
- [29] W. D. Myers and W. J. Swiatecki, *Nucl. Phys.* **81**, 1 (1966).
- [30] W. D. Myers and W. J. Swiatecki, *Ark. Fys.* **36**, 343 (1967).
- [31] J. Töke and W. J. Swiatecki, *Nucl. Phys. A* **372**, 141 (1981).
- [32] W. Reisdorf, *Z. Phys. A* **300**, 227 (1981).
- [33] M. Prakash, J. Wambach, and Z. Y. Ma, *Phys. Lett. B* **128**, 141 (1983).
- [34] S. Shlomo, *Nucl. Phys. A* **539**, 17 (1992).
- [35] J. P. Lestone, *Phys. Rev. C* **52**, 1118 (1995).
- [36] J. P. Lestone, J. R. Leigh, J. O. Newton, D. J. Hinde, J. X. Wei, J. X. Chen, S. Elfström, and M. Zielinska-Pfabé, *Nucl. Phys. A* **559**, 277 (1993).
- [37] J. E. Lynn, in *The Theory of Neutron Resonance Reactions* (Clarendon, Oxford, 1968), p. 325.
- [38] V. G. Nedoresov and Yu. N. Ranyuk, *Fotodelenie Yader za Gigantskim Rezonansom* (Naukova Dumka, Kiev, 1989) (in Russian).
- [39] A. Bohr and B. R. Mottelson, *Nuclear Structure* (Benjamin, New York, 1975), Vols. I and II.
- [40] R. Vandenbosch and J. R. Huizenga, *Nuclear Fission* (Academic, New York, 1973).
- [41] A. Bohr, in *Proceedings of the United Nations International Conference on the Peaceful Uses of Atomic Energy* (United Nations, New York, 1956), Vol. 2, p. 151.
- [42] I. Halpern and V. M. Strutinsky, in *Proceedings of the United Nations International Conference on the Peaceful Uses of Atomic Energy* (United Nations, Geneva, 1958), Vol. 15, p. 408.
- [43] W. Ye, H. W. Yang, and F. Wu, *Phys. Rev. C* **77**, 011302(R) (2008).
- [44] B. Jurado, C. Schmitt, K.-H. Schmidt, J. Benlliure, T. Enqvist, A. R. Junghans, A. Kelić, and F. Rejmund, *Phys. Rev. Lett.* **93**, 072501 (2004).
- [45] F. Videbaek, R. B. Goldstein, L. Grodzins, S. G. Steadman, T. A. Belote, and J. D. Garrett, *Phys. Rev. C* **15**, 954 (1997).
- [46] M. Ogihara, H. Fujiwara, S. C. Jeong, W. Galster, S. M. Lee, Y. Nagashima, T. Mikumo, H. Ikezoe, K. Ideno, Y. Sugiyama, and Y. Tomita, *Z. Phys. A* **335**, 203 (1990).
- [47] D. P. Singh, P. P. Singh Unnati, A. Yadav, M. K. Sharma, B. P. Singh, K. S. Golda, R. Kumar, A. K. Sinha, and R. Prasad, *Phys. Rev. C* **80**, 014601 (2009).
- [48] V. Singh, B. R. Behera, M. Kaur, A. Jhingan, P. Sugathan, S. Pal, D. Siwal, M. Oswal, K. P. Singh, S. Goyal, A. Saxena, and S. Kaila, *EPJ Web Conf.* **86**, 00052 (2015).
- [49] V. Singh, B. R. Behera, M. Kaur, A. Kumar, K. P. Singh, N. Madhavan, S. Nath, J. Gehlot, G. Mohanto, A. Jhingan, I. Mukul, T. Varughese, J. Sadhukhan, S. Pal, S. Goyal, A. Saxena, S. Santra, and S. Kailas, *Phys. Rev. C* **89**, 024609 (2014).
- [50] C. R. Morton, D. J. Hinde, J. R. Leigh, J. P. Lestone, M. Dasgupta, J. C. Mein, J. O. Newton, and H. Timmers, *Phys. Rev. C* **52**, 243 (1995).
- [51] R. N. Sagaidak, V. I. Chepigin, A. P. Kabachenko, A. Yu. Lavrentev, O. N. Malyshev, Yu. Ts. Oganessian, A. G. Popeko, J. Rohac, A. V. Yerebin, S. Hofmann, F. P. Heßberger, V. Ninov, and C. Stodel, in *Proceedings of VI International School-Seminar "Heavy Ion Physics," Dubna, 1997*, edited by Yu. Ts. Oganessian and R. Kalpakchieva (World Scientific, Singapore, 1998), p. 323.

- [52] B. B. Back, R. R. Betts, J. E. Gindler, B. D. Wilkins, S. Saini, M. B. Tsang, C. K. Gelbke, W. G. Lynch, M. A. McMahan, and P. A. Baisden, *Phys. Rev. C* **32**, 195 (1985).
- [53] K. Nishio, H. Ikezoe, Y. Nagame, M. Asai, K. Tsukada, S. Mitsuoka, K. Tsuruta, K. Satou, C. J. Lin, and T. Ohsawa, *Phys. Rev. Lett.* **93**, 162701 (2004).
- [54] B. Behera, S. Roy, P. Basu, M. K. Sharan, S. Jena, M. Satpathy, M. L. Chatterjee, and S. K. Datta, *Pramana, J. Phys.* **57**, 199 (2001).
- [55] V. Singh, B. R. Behera, M. Kaur, D. Siwal, S. Goyal, P. Sugathan, K. S. Golda, A. Jhingan, A. Kumar, A. Saxena, R. K. Bhowmik, and S. Kailas, *EPJ Web Conf.* **17**, 16014 (2011).
- [56] H. Rossner, D. J. Hinde, J. R. Leigh, J. P. Lestone, J. O. Newton, J. X. Wei, and S. Elfström, *Phys. Rev. C* **45**, 719 (1992).
- [57] É. M. Kozulin, A. Ya. Rusanov, and G. N. Smirenkin, *Phys. At. Nucl.* **56**, 166 (1993).
- [58] E. Vulgaris, L. Grodzins, S. G. Steadman, and R. Ledoux, *Phys. Rev. C* **33**, 2017 (1986).
- [59] L. C. Vaz, D. Logan, E. Duck, J. M. Alexander, M. F. Rivet, M. S. Zisman, M. Kaplan, and J. W. Ball, *Z Phys. A* **315**, 169 (1984).
- [60] D. J. Hinde, M. Dasgupta, J. R. Leigh, J. C. Mein, C. R. Morton, J. O. Newton, and H. Timmers, *Phys. Rev. C* **53**, 1290 (1996).
- [61] K.-T. Brinkmann, A. L. Caraley, B. J. Fineman, N. Gan, J. Velkovska, and R. L. McGrath, *Phys. Rev. C* **50**, 309 (1994).